DUAL-CORE SIDE-HOLE FIBER FOR PRESSURE SENS-ING BASED ON INTENSITY DETECTION

D. Chen and G. Hu

Institute of Information Optics Zhejiang Normal University, Jinhua 321004, China

M.-L. V. Tse and H. Y. Tam

Photonics Research Centre, Department of Electrical Engineering The Hong Kong Polytechnic University Hung Hom, Kowloon, Hong Kong SAR, China

Abstract—We propose a novel dual-core side-hole fiber (DCSHF) for air/hydrostatic pressure sensing. Two large air holes are employed in the cross-section of the DCSHF, which result in a difference of the pressure-induced index changes for two fiber cores. The mode coupling between two fiber cores of the DCSHF is sensitive to the pressure-induced index change which ensures the intensity detection of the DCSHF-based pressure sensor. A segment of DCSHF with a length equal to the coupling length of the mode coupling between two fiber cores is used as a pressure sensor. When the light is injected into the central fiber core of the DCSHF, there is a one-to-one correspondence between the pressure and the output power on the output side of the central fiber core. A pressure sensor based on a typical DCSHF can achieve a pressure measurement range of 27 MPa. DCSHFs with different structure parameters for pressure sensing are investigated.

1. INTRODUCTION

Optical fiber based pressure sensors have attracted considerable attentions for several decades due to their advantages such as small size, good reproducibility, long-term stability, fiber compatibility, immunity to electromagnetic interference, etc. Early in 1979, Budiansky et al. discussed the pressure sensitivity of a clad optical

fiber [1]. Later, several pressure sensors based on birefringent fibers were reported [2–6]. Side-hole fibers (SHFs) based on a built-in transducing mechanism to enhance the sensitivity were proposed and demonstrated for pressure sensing [7–12]. It is well known that microstructured fibers (MSFs) or photonic crystal fibers [13–18] have been well-developed in past several years. More recently, several MSFs with the design principle of the SHF were also proposed for pressure sensing [19–24]. Most previously reported optical fiber based pressure sensors are based on demodulation methods such as the birefringence measurement based on a complex setup by using non-fiber components [7–11] which suffers from the high cost, or the optical spectrum detection based on the all fiber interferometer [21–24] which needs costly equipments such as optical spectrum analyzer and also results in a long responding time for pressure sensing.

In this paper, to the best of our knowledge, it is the first time that a dual-core side-hole fiber (DCSHF) which combines both side holes and two fiber cores in the cross-section is proposed for air/hydrostatic pressure sensing. The mode coupling between two fiber cores of the DCSHF is sensitive to the pressure-induced index change, which shows a one-to-one correspondence between the pressure and the output power on the output side of the central fiber core of the DCSHF and the pressure can be measured by using only a Photodiode (PD) based on intensity detection. The DCSHF-based pressure sensor has potential advantages of fiber compatibility, low cost, fast response compared with most optical fiber pressure sensors based on previously reported demodulation methods.

2. DCSHF STRUCTURE AND SENSING MECHANISM

Figure 1(a) shows the cross-section of the proposed DCSHF with a diameter (D), where a pair of large air holes with a radius (R) and a distance (L) are employed to enhance the pressure sensitivity of the DCSHF. The DCSHF has two fiber cores (a and b) with a diameter (d) and a center-to-center distance (H), and the central fiber core a locates in the center of the DCSHF. For a DCSHF-based pressure sensor, a segment of the DCSHF is spliced into two segments of single mode fibers (SMFs) by matching the central fiber core a to the fiber core of the two SMFs.

The operation principle of the pressure sensor can be simply understood as follows. Part of the light injected to the central fiber core a of the DCSHF will be transferred to the fiber core b due to the mode coupling of two fiber cores. The pressure utilized on the DCSHF results in the change of the index and the mode coupling,

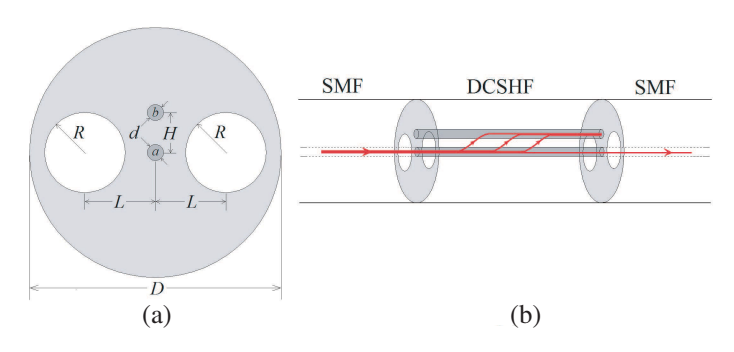


Figure 1. (a) Cross-section of the DCSHF. (b) Schematic diagram of pressure sensor based on the DCSHF.

which means the output power on the output side of the central fiber core a depends on the utilized pressure. For a detailed description, here we briefly introduce some results of the mode coupling theory for the proposed DCSHF, where one can find details in the reference paper [25]. The DCSHF has two basic modes with the effective index (n_e) for the even mode and the effective index (n_o) for the odd mode. Suppose that the power of the injected light on input (left) sides of the central fiber core a and the fiber core b is 1 and 0, respectively. The output power on output (right) sides of the central fiber core a and the fiber core b of the DCSHF with a length (z) can be given by $P_1(z) = \cos^2(Sz) + \cos^2(\eta)\sin^2(Sz)$ and $P_2(z) = \sin^2(\eta)\sin^2(Sz)$, respectively. The maximum power transferred from the central fiber core a to the fiber core b is $P_2|_{\text{max}} = \sin^2(\eta)$ which occurs at the coupling length $z = L_c = \pi/(2S)$. Note that we have $S = |n_e - n_o|\pi/\lambda$, $S = \sqrt{\delta^2 + \kappa^2}$, $\tan(\eta) = \kappa/\delta$, and $\delta = |n_a - n_b|\pi/\lambda$, where n_a and n_b are the effective index of the individual fiber core a and the individual fiber core b (formed waveguides), respectively. Fig. 2 shows calculated mode profiles of the electric field and the electric field distribution along the perpendicular radial direction for the even mode (a) and the odd mode (b) of the DCSHF with the parameters of $H = 20 \,\mu\text{m}$, $L = 35 \,\mu\text{m}$, $R=20 \,\mu\text{m}, d=8 \,\mu\text{m}$ and $D=125 \,\mu\text{m}$ when the operation wavelength is $\lambda = 1550 \, \mathrm{nm}$. Note that refractive indexes of the pure silica and air are assumed to be 1.444 and 1, respectively and the refractive index difference (ID) between the pure silica and two fiber cores is set to be 0.3% for the calculation based on the full-vector finite-element method (FEM). The calculated effective indexes are $n_e = 1.4455383955$ and $n_0 = 1.4455089889$ for the even mode and the odd mode of the DCSHF when it is under no pressure, which indicates the coupling length of $L_c = 2.64 \, \text{cm}.$

When the DCSHF is under an air/hydrostatic pressure, the stress

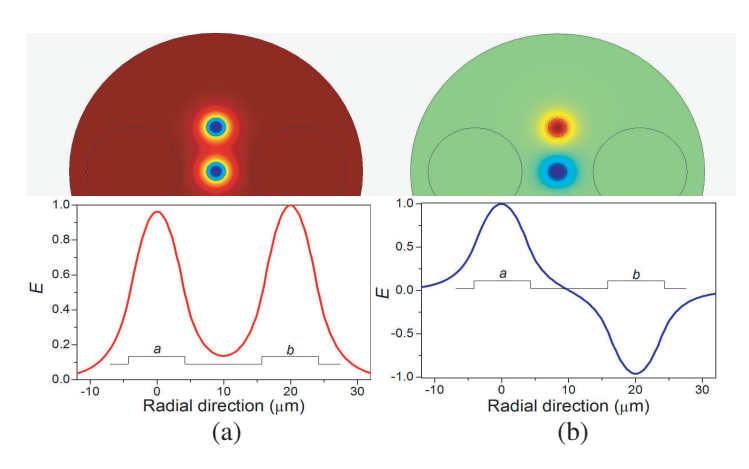


Figure 2. Mode profiles of the electric field and the electric field distribution along the perpendicular radial direction for the even mode (a) and the odd mode (b) of the proposed DCSHF.

in the cross-section of the DCSHF will result in a refractive index change due to the photoelastic effect. The refractive index under the pressure is given by [26] $n_x = n_0 - C_1\sigma_x - C_2(\sigma_y + \sigma_z)$ and $n_y = n_0 - C_1\sigma_y - C_2(\sigma_x + \sigma_z)$, where σ_x , σ_y and σ_z are the stress components, $C_1 = 6.5 \times 10^{-13} \,\mathrm{m}^2/\mathrm{N}$ and $C_2 = 4.2 \times 10^{-12} \,\mathrm{m}^2/\mathrm{N}$ are the stress-optic coefficients for the pure silica. The pressure-induced index change is $\Delta n_x = n_x - n_0 = -C_1\sigma_x - C_2(\sigma_y + \sigma_z)$ and $\Delta n_y = n_y - n_0 = -C_1\sigma_y - C_2(\sigma_x + \sigma_z)$. We also use the FEM to calculate the stress distribution of the DCSHF under the pressure. The Young's modulus $E_{SiO2} = 73.1 \,\mathrm{Gpa}$ and Poisson's ratio $v_{SiO2} = 0.17 \,\mathrm{for}$ the pure silica (and fiber cores) are used in our calculations.

Figure 3 shows the distribution of the principal stress component σ_x (a) and the principal stress component σ_y (b) when the DCSHF is under an air/hydrostatic pressure of 1 MPa. Evidently, there is a relatively large difference for the values of σ_y in the fiber core a region and the fiber core b region, which results in a relatively difference of Δn_x in the fiber core a region and the fiber core b region. Fig. 3(c) shows the pressure-induced index change of the DCSHF, where we can find the pressure-induced index changes are $\Delta n_x = 8.3401 \times 10^{-6}$ and $\Delta n_x = 6.4047 \times 10^{-6}$ in the centers of the fiber core a and the fiber core b. The difference of the pressure-induced index changes in two fiber cores means that the values of δ and S are dependent the pressure which consequently results in the dependence between the pressure and the output power on the output side of the central fiber core a when the length of the DCSHF is a constant.

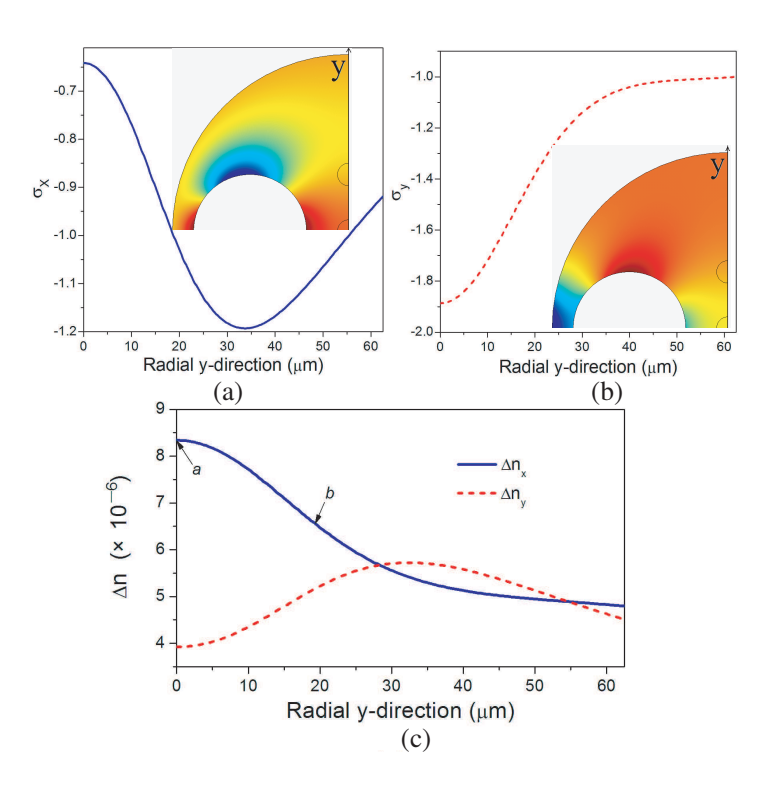


Figure 3. (a) Distribution of the principal stress component σ_x . (b) Distribution of the principal stress component σ_y . (c) Pressure-induced index change of the DCSHF.

3. PERFORMANCE OF THE DCSHF-BASED PRESSURE SENSOR

A segment of 2.64-cm DCSHF with the parameters of ID=0.3%, $H=20\,\mu\mathrm{m},\ L=35\,\mu\mathrm{m},\ R=20\,\mu\mathrm{m},\ d=8\,\mu\mathrm{m}$ and $D=125\,\mu\mathrm{m}$ is used as the pressure sensor. We calculate the power (solid curve in Fig. 4(a)) on the output side of the central fiber core a and the power (dotted curve in Fig. 4(a)) transferred from the central fiber core a to the fiber core b when the 2.64-cm DCSHF is under different pressure. Note that the injected power of the x-polarized light in the central fiber core a is supposed to be 1. Fig. 4(b) shows the normalized electric field distribution along the perpendicular radial direction for the even modes of the proposed DCSHF under the air/hydrostatic pressure of 0 MPa, 5 MPa, 15 MPa, 30 MPa, 40 MPa, corresponding to A, B, C, D, E points in Fig. 4(a). The maximum power transfered

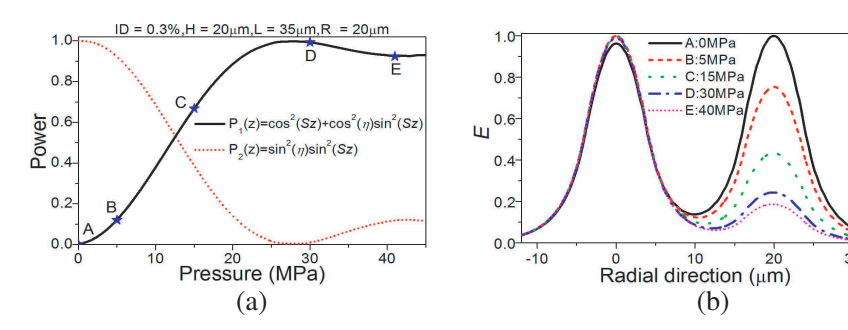


Figure 4. (a) Power on the output side of the central fiber core a (solid curve) and power transferred (dotted curve) from fiber core a to fiber core b. (b) Normalized electric field distribution along the perpendicular radial direction for the even modes of the proposed DCSHF under different air/hydrostatic pressure.

from fiber core a to fiber core b has a monotonic decrease when the pressure increases. When the length of the DCSHF is $L_c = 2.64 \,\mathrm{cm}$, the output power at the output of the central fiber core a is up to ~ 1 when the air/hydrostatic pressure is 27 MPa. We can find a one-to-one correspondence between the pressure and the output power when the pressure is less than 27 MPa, which indicates the measurement range of the pressure sensor based on the 2.64-cm DCSHF is 27 MPa. The sensitivity is about 6%/Mpa when the output power is around 0.5.

Figure 5 shows the output power on the output side of the cental fiber core a of the DCSHFs with structure parameters of (ID = 0.4%, $H = 20 \,\mu\text{m}, L = 35 \,\mu\text{m}, R = 20 \,\mu\text{m}, (ID = 0.3\%, H = 20 \,\mu\text{m})$ $L = 30 \,\mu\text{m}, R = 20 \,\mu\text{m}, (ID = 0.3\%, H = 24 \,\mu\text{m}, L = 35 \,\mu\text{m},$ $R = 20 \,\mu\text{m}$), and $(ID = 0.3\%, H = 20 \,\mu\text{m}, L = 35 \,\mu\text{m}, R = 15 \,\mu\text{m})$. Note that the length of each DCSHF is equal to the coupling length between the two fiber cores and other parameters are $d = 8 \,\mu\mathrm{m}$ and $D = 125 \,\mu\text{m}$. Fig. 5(a) shows that the DCSHF with a larger index difference has a higher pressure sensitivity (about 14%/MPa for the output power of 0.5) and a smaller measurement range (about 11 MPa) compared with the 2.64-cm DCSHF discussed above. The DCSHF with a larger index difference has a longer coupling length between the two fiber cores due to a smaller initial value of S, which results to a higher pressure sensitivity and a smaller measurement range. For DCSHFs with structure parameters of $(ID = 0.3\%, H = 20 \,\mu\text{m}, L = 30 \,\mu\text{m})$ $R = 20 \,\mu\text{m}$), two large air holes are close to the central fiber core a which results in a large initial value of δ . The utilized pressure will decrease the value of δ which play a crucial role to increase the output power transferred from the central fiber core a to the fiber core b when

the pressure increases. Thus, our calculations show that the output power at the central fiber core a decreases when the pressure increases in Fig. 5(b) where the output power is only 0.415 when the pressure is 0 MPa. Fig. 5(c) shows that the DCSHF with two long-distance fiber cores also has a higher pressure sensitivity (about 23%/MPa for the output power of 0.5) and a smaller measurement range (about 7 MPa). Fig. 5(d) shows that the DCSHF with two smaller air holes has a lower pressure sensitivity (about 4.8%/MPa for the output power of 0.5) and a larger measurement range (about 32 MPa) due to the smaller pressure-induced change of the value of S. The above simulations show that the DCSHF-based pressure sensors with different sensitivities or measurement ranges can be achieved based on the designs of the DCSHF.

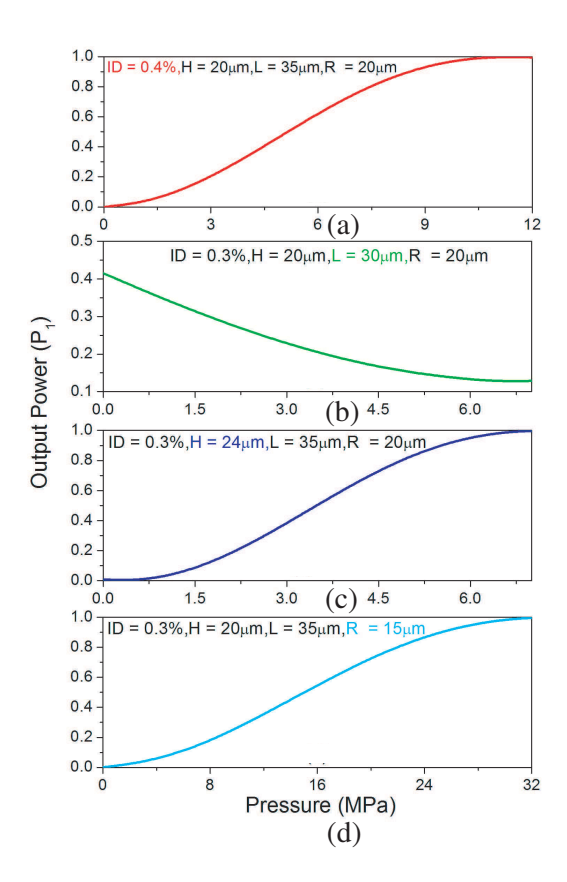


Figure 5. Outuput power on the output side of the central fiber core a of the DCSHFs with different structure parameters.

4. CONCLUSION

In conclusion, we have proposed a DCSHF with two large air holes and two fiber cores in the cross-section using as a kind of air/hydrostatic pressure sensor. A segment of the DCSHF with a length equal to the coupling length of two fiber cores can be used as a pressure sensor based on the intensity detection when the DCSHF is spliced to two segments of SMFs by matching the central fiber core a to the fiber core of SMFs. The operation principle of the DCSHF-based pressure sensor has been presented. In details a segment of 2.64-cm DCSHF with the parameters of ID=0.3%, $H=20\,\mu\text{m}$, $L=35\,\mu\text{m}$, $R=20\,\mu\text{m}$, $d=8\,\mu\text{m}$ and $D=125\,\mu\text{m}$ using as a pressure sensor with a measurement range of 27 MPa and a sensitivity of 6%/MPa when the output power is around 0.5 has been investigated. Other DCSHFs with different structure parameters have also been investigated, which indicates DSCHF based pressure sensors with different sensitivities or measurement ranges can be achieved based on the designs of the DCSHF.

ACKNOWLEDGMENT

This work is supported by the Natural Science Foundation of China under project (No. 61007029) and the Central Research Grant of The Hong Kong Polytechnic University under the Postdoctoral Fellowship (Project No. G-YX2D).

REFERENCES

- 1. Budiansky, B., D. C. Drucker, G. S. Kino, and J. R. Rice, "Pressure sensitivity of a clad optical fiber," *Appl. Opt.*, Vol. 18, 4085–4088, 1979.
- 2. Bock, W. J. and A. W. Domanski, "High hydrostatic pressure effects in highly birefringent optical fibers," *J. Lightwave Technol.*, Vol. 7, 1279–1283, 1989.
- 3. Chiang, K. S. and D. Wong, "Hydrostatic pressure-induced birefringence in a highly birefringent optical fiber," *Electron. Lett.*, Vol. 26, 1952–1954, 1990.
- 4. Wang, A., S. He, X. Fang, X. Jin, and J. Lin, "Optical fiber pressure sensor based on photoelasticity and its application," <u>J. Lightwave Technol.</u>, Vol. 10, 1466–1472, 1992.
- 5. Wolinski, T. R. and W. J. Bock, "Birefringence measurement under hydrostatic pressure in twisted highly birefringent fibers," *IEEE Trans. Instrum. Meas.*, Vol. 44, No. 3, 708–711, 1995.

- 6. Ma, J., W. Tang, and W. Zhou, "Optical-fiber sensor for simultaneous measurement of pressure and temperature: Analysis of cross sensitivity," *Appl. Opt.*, Vol. 35, 5206–5210, 1996.
- 7. Xie, H. M., Ph. Dabkiewicz, and R. Ulrich, "Side-hole fiber for fiber-optic pressure sensing," *Opt. Lett.*, Vol. 11, 333–335, 1986.
- 8. Charasse, M. N., M. Turpin, and J. P. Le Pesant, "Dynamic pressure sensing with a side-hole birefringent optical fiber," *Opt. Lett.*, Vol. 16, 1043–1045, 1991.
- 9. Clowes, J. R., S. Syngellakis, and M. N. Zervas, "Pressure sensitivity of side-hole optical fiber sensors," *IEEE Photon. Technol. Lett.*, Vol. 10, 857–859, 1998.
- 10. Zhao, Y. and F. Ansari, "Instrinsic single-mode fiber-optic pressure sensor," *IEEE Photon. Technol. Lett.*, Vol. 13, 1212–1214, 2001.
- 11. Nawrocka, M. S., W. J. Bock, and W. Urbanczyk, "Dynamic high-pressure calibration of the fiber-optic sensor based on birefringent side-hole fibers," *J. Sens.*, Vol. 5, 1011–1018, 2005.
- 12. Frazao O., S. O. Silva, J. M. Baptista, J. L. Santos, G. Statkiewicz-Barabach, W. Urbanczyk, and J. Wojcik, "Simultaneous measurement of multiparameters using a Sagnac interferometer with polarization maintaining side-hole fiber," *Appl. Opt.*, Vol. 47, 4841–4848, 2008.
- Knight, J. C., T. A. Birks, P. St. J. Russell, and D. M. Atkin, "All-silica single-mode optical fiber with photonic crystal cladding," Opt. Lett., Vol. 21, 1547–1549, 1996.
- 14. Knight, J. C., "Photonic crystal fibers," Nature, Vol. 424, 847–851, 2003.
- 15. Nozhat, N. and N. Granpayeh, "Specialty fibers designed by photonic crystals," *Progress In Electromagnetics Research*, Vol. 99, 225–244, 2009.
- 16. Chen, D., M.-L. Vincent Tse, and H.-Y. Tam, "Optical properties of photonic crystal fibers with a fiber core of arrays of subwavelength circular air holes: birefringence and dispersion," *Progress In Electromagnetics Research*, Vol. 105, 193–212, 2010.
- 17. Li, J., J. Wang, and F. Jing, "Improvement of coiling mode to suppress higher-order-modes by considering mode coupling for large-mode-area fiber laser," *Journal of Electromagnetic Waves and Applications*, Vol. 24, No. 8–9, 1113–1124, 2010.
- 18. Shen, G.-F., X.-M. Zhang, H. Chi, and X.-F. Jin, "Microwave/millimeter-wave generation using multi-wavelength photonic crystal fiber brillouin laser," *Progress In Electromagnet*-

- ics Research, Vol. 80, 307-320, 2008.
- 19. Statkiewicz, G., T. Martynkien, and W. Urbanczyk, "Measurements of modal birefringence and polarimetric sensitivity of the birefringent holey fiber to hydrostatic pressure and strain," *Opt. Communications*, Vol. 241, 339–348, 2004.
- 20. Szpulak, M., T. Martynkien, and W. Urbanczyk, "Effects of hydrostatic pressure on phase and group modal birefringence in microstructured holey fibers," *Appl. Opt.*, Vol. 43, 4739–4744, 2004.
- Fu, H. Y., H. Y. Tam, L. Y. Shao, X. Dong, P. K. A. Wai, C. Lu, and S. K. Khijwania, "Pressure sensor realized with polarization-maintaining photonic crystal fiber-based Sagnac interferometer," *Appl. Opt.*, Vol. 47, 2835–2839, 2008.
- 22. Szczurowski, M. K., T. Martynkien, G. Statkiewicz-Barabach, W. Urbanczyk, and D. J. Webb, "Measurements of polarimentric sensitivity to hydrostatic pressure, strain and temperature in birefringent dual-core microstructured polymer fiber," *Opt. Express*, Vol. 18, 12076–12087, 2010.
- 23. Martynkien, T., G. Statkiewicz-Barabach, J. Olszewski, J. Wojcik, P. Mergo, T. Geernaert, C. Sonnenfeld, A. Anuszkiewicz, M. K. Szczurowski, K. Tarnowski, M. Makara, K. Skorupski, J. Klimek, K. Poturaj, W. Urbanczyk, T. Nasilowski, F. Berghmans, and H. Thienpont, "Highly birefringent microstructured fibers with enhanced sensitivity to hydrostatic pressure," Opt. Express, Vol. 18, 15113–15121, 2010.
- 24. Kim, H. M., T. H. Kim, B. Kim, and Y. Chung, "Enhanced transverse load sensitivity by using a highly birefringent photonic crystal fiber with larger air holes on one axis," *Appl. Opt.*, Vol. 49, 3841–3845, 2010.
- 25. Huang, W. P., "Coupled-mode theory for optical waveguides: An overview," J. Opt. Soc. Am. A, Vol. 11, 963–983, 1994.
- 26. Wu, C., B. O. Guan, Z. Wang, and X. Feng, "Characterization of pressure response of Bragg gratings in grapefruit microstructured fibers," *J. Lightwave Technol.*, Vol. 28, 1392–1397, 2010.